Pilot-Based Estimation of Time-Varying Multipath Channels for Coherent CDMA Receivers

Marc-Antoine R. Baissas and Akbar M. Sayeed, *Member, IEEE*

***Abstract*—Reliable coherent wireless communication requires accurate estimation of the time-varying multipath channel. This paper addresses two issues in the context of direct-sequence code-division multiple access (CDMA) systems: i) linear minimum-mean-squared-error (MMSE) channel estimation based on a pilot transmission and ii) impact of channel estimation errors on coherent receiver performance. A simple characterization of the MMSE estimator in terms of a bank of filters is derived. A key channel characteristic controlling system performance is the normalized coherence time, which is approximately the number of symbols over which the channel remains strongly correlated. It is shown that the estimator performance is characterized by an effective signal-to-noise ratio (SNR)—the product of the pilot SNR and the normalized coherence time. A simple uniform averaging estimator is also proposed that is easy to implement and delivers near-optimal performance if properly designed. The receivers analyzed in this paper are based on a time–frequency RAKE structure that exploits joint multipath-Doppler diversity. It is shown that the overall receiver performance is controlled by two competing effects: shorter coherence times lead to degraded channel estimation but improved inherent receiver performance due to Doppler diversity, with opposite effects for longer coherence times. Our results demonstrate that exploiting Doppler diversity can significantly mitigate the error probability floors that plague conventional CDMA receivers under fast fading due to errors in channel estimation.**

***Index Terms*—Doppler diversity, fast fading, MMSE estimation, RAKE receivers.**

I. Introduction

MOBILE wireless channels are characterized by time-varying multipath propagation effects, and accurate channel estimation is critical to reliable coherent communication [1], [2]. Indeed, emerging wireless standards accommodate pilot signal transmissions dedicated to channel estimation [3], [4]. In this paper, we address time-varying channel estimation for spread-spectrum code-division multiple access (CDMA) systems that have emerged as a promising core wireless technology. Our focus is primarily on single-user systems employing short codes.[1] We develop a framework for designing pilot-based linear MMSE channel estimators and for assessing the impact of estimation errors on receiver performance. Our framework is based on a canonical linear channel model that captures the essential degrees of freedom in the channel in terms of a fixed basis. The fixed basis waveforms are defined by uniformly spaced delays and Doppler shifts of the signaling waveform [5]–[8]. Unlike other existing models for time-varying channels (see, e.g., [9]–[11]), the canonical model eliminates the need for estimating actual physical delays and Doppler shifts encountered during propagation—channel estimation boils down to estimating the multipath-Doppler expansion coefficients with respect to the fixed basis that characterize the effects of the channel.

We consider both time– and frequency-selective channels and provide simple characterizations of the optimal estimator in terms of a bank of filters, each associated with a particular multipath-Doppler channel component. We show that the key parameter controlling the estimator performance is an *effective signal-to-noise ratio (SNR)*, which is the product of the pilot SNR and the channel *coherence time* normalized by the symbol duration. The coherence time Δt_c is the duration over which the channel coefficients remain strongly correlated [1], [2]. Essentially, Δt_c limits the duration over which time averaging can be done to reduce the effects of noise. Thus, longer coherence times improve the effective SNR and, hence, the estimator performance. We also consider a simple suboptimal estimator—uniform averager—that is particularly easy to implement. We show that a properly designed uniform averager delivers near-optimal performance.

Channel estimation errors incurred due to the relatively small Δt_c in fast fading scenarios have a significant impact on the performance of coherent CDMA RAKE receivers [12]–[16]. As reported in several studies (see, e.g., [12]–[15]), the conventional RAKE receiver exhibits a bit-error-probability (BEP) floor due to degraded channel estimation in such conditions. While shorter coherence times (large Doppler spreads) degrade channel estimation, it was shown in [5] that they can be exploited for additional diversity—Doppler diversity—via a time-frequency RAKE receiver structure. Consequently, when joint multipath-Doppler diversity is exploited, the overall receiver performance is controlled by these competing effects. The results reported here show that at low pilot SNRs, channel estimation errors dominate, resulting in degraded performance at shorter coherence times (faster fading), which is consistent with existing studies. However, in contrast to the conventional RAKE receiver, at sufficiently high pilot SNRs, the effects of Doppler diversity can dominate, resulting in improved receiver performance under fast fading. Consequently, at sufficiently high pilot

Manuscript received April 12, 2000; revised April 8, 2002. This work was supported in part by Wisconsin Alumni Research Foundation and by the National Science Foundation under Grants CCR-9875805 and ECS-9979448. The associate editor coordinating the review of this paper and approving it for publication was Prof. Dimitrios Hatzinakos.

M.-A. R. Baissas is with Texas Instruments, Inc., Dallas, TX 75243 USA.

A. M. Sayeed is with the Department of Electrical and Computer Engineering, University of Wisconsin, Madison, WI 53706 USA (e-mail: akbar@engr.wisc.edu).

Publisher Item Identifier 10.1109/TSP.2002.800400.

[1]Section VI briefly discusses extensions to long codes and multiuser systems.

SNRs, time–frequency RAKE receivers can significantly mitigate the BEP floors that plague the performance of conventional RAKE receivers.

The next section describes the canonical channel model underlying our framework. Section III develops useful representations for the linear MMSE estimator and discusses design rules for the uniform averager. Section IV analyzes the performance of the estimators. Section V studies the impact of channel estimation errors on receiver performance. Numerical results are presented to illustrate the estimator and receiver performance under a variety of conditions. Section VI briefly discusses some extensions, including multiuser systems and long codes. Concluding remarks are presented in Section VII.

II. Signal and Channel Models

The complex baseband signal $x(t)$ at the output of a mobile wireless channel is related to the transmitted complex baseband waveform $s(t)$ by the relation [2]

$$x(t) = \int_0^{T_m} h(t, \tau) s(t-\tau)\, d\tau \tag{1}$$

where $h(t, \tau)$ is the time-varying impulse response of the channel. The maximum delay is denoted by T_m, which is the *multipath spread* of the channel. An equivalent representation of $x(t)$, which clearly shows temporal and spectral dispersion, is [2], [6]

$$x(t) = \int_0^{T_m} \int_{-B_d}^{B_d} H(\theta, \tau) s(t-\tau) e^{j2\pi\theta t}\, d\theta\, dt, \tag{2}$$

$$H(\theta, \tau) = \int h(t, \tau) e^{-j2\pi\theta t}\, dt \tag{3}$$

where the channel is characterized by the multipath-Doppler *spreading function* $H(\theta, \tau)$. The maximum Doppler frequency is denoted by B_d, which is the *Doppler spread* of the channel. A discrete version of (2) is often used in practice (see, for e.g., [9]) to model dominant propagation paths

$$x(t) = \sum_{l=1}^{L_T} \beta_l s(t-\tau_l) e^{j2\pi\theta_l t} \tag{4}$$

where L_T denotes the total number of paths, and the lth path is associated with delay $\tau_l \in [0, T_m]$, Doppler shift $\theta_l \in [-B_d, B_d]$, and fading gain β_l.

For statistical channel characterization, the wide-sense stationary uncorrelated scatterer (WSSUS) model [1], [6], [2] is widely used in practice in which the temporal variations in $h(t, \tau)$ are represented as a stationary Gaussian process, and the channel responses at different lags are uncorrelated. For a zero-mean channel (Rayleigh fading[2]), the second-order statistics are given by

$$\mathrm{E}[H(\theta, \tau) H^*(\theta', \tau')] = \Psi(\theta, \tau)\delta(\theta-\theta')\delta(\tau-\tau') \tag{5}$$

where $\delta(.)$ denotes the Dirac delta function, and $\Psi(\theta, \tau)$ is the multipath-Doppler *scattering function* [2], [6] that characterizes the channel statistics and quantifies the channel power density at different multipath delays and Doppler frequencies. The overall noisy signal at the receiver is given by

$$r(t) = x(t) + n(t) \tag{6}$$

where $n(t)$ is zero-mean complex additive white Gaussian noise (AWGN).

A. Canonical Channel Representation

Physical channel modeling, as exemplified by the discrete model (4), requires estimation of the delays (τ_l), Doppler shifts (θ_l), and fading coefficients (β_l) associated with each path. The canonical channel characterization [5], [6], [8], [7], on the other hand, eliminates the need for (nonlinear) estimation of delays and Doppler shifts by exploiting the fact that the receiver has limited resolution in frequency and time due to the finite duration T and (essentially) finite bandwidth B, respectively, of the symbol signaling waveform $s(t)$. More specifically, the canonical representation asserts that the received signal $x(t)$ can be represented arbitrarily accurately in terms of *fixed*, uniformly spaced multipath delays and Doppler shifts of the transmitted symbol waveform [5]–[8]

$$x(t) \approx \sum_{n=0}^{N} \sum_{k=-K}^{K} h_{k,n} s\left(t - \frac{n}{B}\right) e^{j(2\pi kt/T)}, \quad 0 \le t \le T \tag{7}$$

where $N \approx \lceil T_m B \rceil$ and $K \approx \lceil T B_d \rceil$ denote the numbers of *resolvable* multipath delays and Doppler frequencies, respectively. We assume that $T_m \ll T$ (negligible intersymbol interference), which is a realistic assumption in CDMA systems.

The above representation states that the received signal is a linear combination of a set of basis waveforms

$$u_{k,n}(t) = s\left(t - \frac{n}{B}\right) e^{j(2\pi kt/T)}, \quad 0 \le t \le T \tag{8}$$

that are *fixed a priori* and do not depend on the actual physical delays and Doppler shifts. For CDMA waveforms with chip duration T_c, chip rate sampling ($B = 1/T_c$) yields an approximately orthogonal basis [5]. Sub-chip-rate oversampling by a factor $\mathcal{O}$ ($B = \mathcal{O}/T_c$) may be used to improve the accuracy of (7) but results in a nonorthogonal basis in general. All information about the channel is linearly represented by the coefficients $\{h_{k,n}\}$, which are samples of a smoothed version of the spreading function [see (12)]. We note that the Doppler coefficients (index k) capture the temporal channel variations *within* the symbol duration T. Temporal channel variations over symbols are captured by the variation of $\{h_{k,n}\}$ over symbols.

The representation (7) also reveals the inherent multipath-Doppler diversity afforded by the channel [5]. The level of diversity is $(N+1)(2K+1) \approx 1+2T_m B_d TB+T_m B+2TB_d \approx 2T_m B_d TB$, which can be increased by increasing T, B or both. Spread-spectrum signaling ($TB \gg 1$) is particularly advantageous for exploiting channel diversity since $T_m B_d \ll 1$ for typical (underspread) channels.

B. Pilot-Based Channel Estimation

We assume that the channel spreads T_m and B_d are known *a priori*. Based on (7), channel estimation thus boils down to estimating $\{h_{k,n}\}$ for each symbol. The representation (7) also

[2]We focus on Rayleigh fading throughout this paper.

dictates projection onto $\{u_{k,n}(t)\}$ as the front-end processing at the receiver

$$z_{k,n} = \langle r, u_{k,n}\rangle = \int_0^T r(t)u_{k,n}^*(t)\,dt. \tag{9}$$

The channel coefficients $\{h_{k,n}\}$ for the symbol of interest are estimated by processing the matched-filter outputs $\{z_{k,n}\}$ over a frame of symbols to exploit the temporal channel correlation. For a WSSUS channel, we can assume the symbol of interest to be the 0th symbol without loss of generality. We assume that a frame of $(2I+1)$ pilot symbols is used to estimate the channel coefficients $\{h_{k,n}\}$ corresponding to the 0th symbol. The received signal corresponding to this frame can be represented as

$$r(t) \approx \sum_{i=-I}^{+I}\sum_{n=0}^{N}\sum_{k=-K}^{K} h_{k,n}(i)u_{k,n}(t-iT) + n(t) \tag{10}$$

where $\{h_{k,n}(i)\}$ are the channel coefficients corresponding to the ith symbol ($iT \le t \le (i+1)T$), and $n(t)$ is zero-mean complex AWGN with power spectral density (PSD) σ_p^2.

The canonical channel coefficients $h_{k,n}(i)$ can be computed as [5], [6]

$$h_{k,n}(i) = \hat{H}_i\left(\frac{k}{T}, \frac{n}{B}\right) \tag{11}$$

$$\begin{aligned}\hat{H}_i(\theta,\tau) &= \int_{iT}^{(i+1)T} h(t,\tau)e^{-j2\pi\theta t}\,dt \\ &= \int_0^{T_m}\int_{-B_d}^{B_d} H(\theta',\tau')e^{-j\pi(\theta-\theta')T}e^{-j2\pi iT(\theta-\theta')} \\ &\quad\cdot \operatorname{sinc}((\theta-\theta')T)\operatorname{sinc}((\tau-\tau')B)\,d\theta'\,d\tau'\end{aligned} \tag{12}$$

where $\operatorname{sinc}(x) = \sin(\pi x)/(\pi x)$. It can be shown that for any particular symbol the different coefficients $\{h_{k,n}(i)\}$ are approximately uncorrelated if the scattering function is sufficiently smooth [5], [6]. Thus, throughout this paper, we assume that for any given i, $\mathrm{E}[h_{k,n}(i)h_{k',n'}^*(i)] = E[\,|h_{k,n}(i)|^2]\,\delta_{n-n'}\,\delta_{k-k'}$, where δ_n denotes the Kronecker delta function. However, the channel is correlated across symbols, and the temporal correlation function for a particular coefficient can be computed using (11) and (12) as

$$\begin{aligned}r_{k,n}(m) &= \mathrm{E}[h_{k,n}(i)h_{k,n}^*(i-m)] \\ &= \int_0^{T_m}\int_{-B_d}^{B_d}\Psi(\theta,\tau)\operatorname{sinc}^2(k-\theta T) \\ &\quad\cdot \operatorname{sinc}^2(n-\tau B)e^{j2\pi\theta mT}\,d\theta\,d\tau.\end{aligned} \tag{13}$$

The frame size parameter I in (10) depends on the channel coherence time Δt_c. While I can be chosen arbitrarily large in the case of optimal estimators,[3] its choice is critical in the case of suboptimal estimators, such as a uniform averager that simply averages the matched-filter outputs $z_{k,n}(i)$ over the frame. Essentially, $2I$ should be on the order of the normalized coherence time $\Delta t_c/T \approx 1/2TB_d$ for suboptimal estimators.

[3]The optimal estimator implicitly averages over an effective frame size commensurate with Δt_c.

For notational convenience, concatenate $\{h_{k,n}(i)\}$ into a $(2K+1)(N+1)$-dimensional vector $\mathbf{h}(i)$. Similarly, define the vector of waveforms $\mathbf{u}(t)$ in terms of the basis waveforms $\{u_{k,n}(t)\}$ in (8). The received signal in (10) can then be compactly expressed as

$$r(t) \approx \sum_{i=-I}^{+I}\mathbf{u}^T(t-iT)\mathbf{h}(i) + n(t). \tag{14}$$

The matched-filtered outputs for each symbol in (9) can be expressed as

$$\mathbf{z}(i) = \langle r(t), \mathbf{u}(t-iT)\rangle = \mathbf{P}\mathbf{h}(i) + \mathbf{w}(i) \tag{15}$$

where $\mathbf{P}$ is a $(2K+1)(N+1)\times(2K+1)(N+1)$ matrix of correlations between different multipath-Doppler basis waveforms

$$\mathbf{P} = \int \mathbf{u}^*(t-iT)\mathbf{u}^T(t-iT)\,dt = \int_0^T \mathbf{u}^*(t)\mathbf{u}^T(t)\,dt \tag{16}$$

and $\mathbf{w}(i)$ is zero-mean vector Gaussian noise with $\mathrm{E}[\mathbf{w}(i)\mathbf{w}(i')^H] = \sigma_p^2\mathbf{P}\delta_{i-i'}$. Note that $\mathbf{P} \approx \mathbf{I}$ for chip-rate sampling ($B = 1/T_c$) and a unit energy signaling waveform $s(t)$.

III. Linear MMSE Channel Estimator

We are interested in estimating $\mathbf{h}(0)$ from the matched-filter outputs $\{\mathbf{z}(i)\colon -I \le i \le I\}$. Let $\mathbf{z} = [\mathbf{z}^T(-I), \ldots, \mathbf{z}^T(I)]^T$ be the $(2I+1)(2K+1)(N+1)\times 1$ vector of matched-filter outputs for the entire frame, which takes the form

$$\mathbf{z} = \mathbf{Q}\mathbf{h} + \mathbf{w} \tag{17}$$

where $\mathbf{h}$ is the concatenated vector corresponding to $\{\mathbf{h}(i)\}$, $\mathbf{w}$ corresponds to $\{\mathbf{w}(i)\}$, and $\mathbf{Q} = \operatorname{diag}(\mathbf{P}, \mathbf{P}, \ldots, \mathbf{P})$ is a $(2I+1)(2K+1)(N+1)\times(2I+1)(2K+1)(N+1)$ block diagonal matrix. Note that $\mathbf{w}$ is a zero-mean Gaussian vector with covariance matrix $\sigma_p^2\mathbf{Q}$.

A linear estimator of $\mathbf{h}(0)$ from $\mathbf{z}$ can be represented as $\hat{\mathbf{h}}(0) = \mathbf{G}^H\mathbf{z}$, where $\mathbf{G}$ is a $(2I+1)(2K+1)(N+1)\times(2K+1)(N+1)$ matrix. The linear MMSE channel estimation problem is thus formulated as

$$\mathbf{G}_{opt} = \arg\min_{\mathbf{G}} \mathrm{E}\left[\|\mathbf{h}(0) - \mathbf{G}^H\mathbf{z}\|^2\right] \tag{18}$$

and the solution is the well-known Wiener filter given by

$$\begin{aligned}\mathbf{G}_{opt} &= \left(\mathrm{E}[\mathbf{z}\mathbf{z}^H]\right)^{-1}\mathrm{E}[\mathbf{z}\mathbf{h}^H(0)] \\ &= \left(\mathbf{Q}\mathrm{E}[\mathbf{h}\mathbf{h}^H]\mathbf{Q} + \sigma_p^2\mathbf{Q}\right)^{-1}\mathbf{Q}\mathrm{E}[\mathbf{h}\mathbf{h}^H(0)] \\ &= \left(\mathrm{E}[\mathbf{h}\mathbf{h}^H]\mathbf{Q} + \sigma_p^2\mathbf{I}\right)^{-1}\mathrm{E}[\mathbf{h}\mathbf{h}^H(0)].\end{aligned} \tag{19}$$

We next investigate the structure of $\mathbf{G}_{opt}$ in special cases to gain more insight. We start with the case of orthogonal basis waveforms.

A. Orthogonal Basis

This case corresponds to chip-rate sampling of the matched-filter outputs, that is, $B = 1/T_c$ in (7). As mentioned earlier, $\mathbf{P} \approx \mathbf{I}$ in this case. Furthermore, since the

different $h_{k,n}$s are uncorrelated, it follows that each $h_{k,n}$ can be estimated separately. For each (k, n), we concatenate the coefficients $\{h_{k,n}(i)\}$ for different symbols into a $(2I+1)$ vector $\mathbf{h}_{k,n}$. Similarly, define $\mathbf{z}_{k,n}$ and $\mathbf{w}_{k,n}$ with $\mathbf{z}_{k,n} = \mathbf{h}_{k,n} + \mathbf{w}_{k,n}$. The estimator for each (k, n) can be expressed as $\hat{h}_{k,n}(0) = \mathbf{g}_{k,n}^H \mathbf{z}_{k,n}$, with the optimal estimator given by

$$\mathbf{g}_{k,n,opt} = (\mathbf{R}_{k,n} + \sigma_p^2 \mathbf{I})^{-1} \mathbf{r}_{k,n} \tag{20}$$

where $\mathbf{R}_{k,n} = \mathrm{E}[\mathbf{h}_{k,n}\mathbf{h}_{k,n}^H]$, and $\mathbf{r}_{k,n} = \mathrm{E}[\mathbf{h}_{k,n}h_{k,n}^*(0)]$. The $(2I+1)$-dimensional cross-correlation vector $\mathbf{r}_{k,n}$ is given by

$$\mathbf{r}_{k,n} = [r_{k,n}(-I), \ldots, r_{k,n}(I)]^T \tag{21}$$

and the elements of the $(2I+1) \times (2I+1)$ correlation matrix $\mathbf{R}_{k,n}$ are given by

$$\mathbf{R}_{k,n}(l, m) = r_{k,n}(l-m), \qquad 1 \le l, m \le 2I+1 \tag{22}$$

where $r_{k,n}(m)$ is given by (13). Due to the Toeplitz structure of $\mathbf{R}_{k,n}$ induced by the WSSUS channel, in the limit of large I, the estimator for each multipath-Doppler channel coefficient can also be interpreted as a linear time-invariant filter $\{g_{k,n,opt}(m)\}$ that acts on the sequence $\{z_{k,n}(i)\}$: $\hat{h}_{k,n}(i) = \sum_{m=-\infty}^{\infty} g_{k,n,opt}(m) z_{k,n}(i-m)$. Consequently, for large I, the estimator also admits a frequency-domain representation $\hat{h}_{k,n}(i) = \int_{-1/2}^{1/2} G_{k,n,opt}(\nu) Z_{k,n}(\nu) e^{j2\pi\nu i}\, d\nu$, where $G_{k,n,opt}(\nu) = \sum_{m=-\infty}^{\infty} g_{k,n,opt}(m) e^{-j2\pi\nu m}$ is the discrete-time Fourier transform (DTFT) of $\{g_{k,n,opt}(m)\}$, and similarly, $Z_{k,n}(\nu)$ is the DTFT of $\{z_{k,n}(i)\}$. The frequency domain representation is depicted in Fig. 1, where the optimal estimator is represented as $G_{k,n,opt}(\nu) = (S_{k,n}(\nu)/S_{k,n}(\nu) + \sigma_p^2)$ in terms of the PSD $S_{k,n}(\nu)$ associated with the correlation sequence $r_{k,n}(m)$: $S_{k,n}(\nu) = \sum_{m=-\infty}^{\infty} r_{k,n}(m) e^{-j2\pi\nu m}$. This is also the eigen-domain representation of the estimator since complex exponentials are the eigenfunctions of (Toeplitz) $\mathbf{R}_{k,n}$ in the limit of large I [17].

B. Nonorthogonal Basis

At chip-rate sampling, there may be some loss in the signal representation (7) due to the bandwidth approximation. As noted earlier, oversampling ($B = \mathcal{O}/T_c$) the matched-filter outputs improves its accuracy. In this case, the corresponding basis waveforms (8) are no longer orthogonal; that is, $\mathbf{P} \neq \mathbf{I}$. However, $\{h_{k,n}\}$ are still approximately uncorrelated if oversampling commensurate with signal bandwidth is employed [5]. In this case, the noise vector $\mathbf{w}(i)$ in (15) has correlated components, and thus, joint processing is needed across multipath-Doppler coordinates as well as across symbols. However, as demonstrated next, with simple pre and postprocessing, this case can be transformed into the simple orthogonal-basis case, where joint processing is needed only across symbols.

In order to derive the estimator structure in this case, we make the mild assumption that the correlation structure in time is identical for different channel coefficients[4]

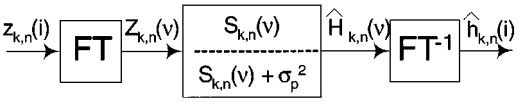

Fig. 1. Frequency-domain Wiener filter representation for the optimum estimator of a particular multipath-Doppler channel coefficient.

$$E[\mathbf{h}(i)\mathbf{h}^H(i')] = r(i-i')\mathbf{\Gamma} \tag{23}$$

where we assume, without loss of generality, that $r(m)$ is the correlation function of the $(k, n) = (0, 0)$ coefficient, and the diagonal matrix $\mathbf{\Gamma}$ denotes the powers in the different coefficients relative to that of the $(0, 0)$th coefficient. Consider the eigendecomposition $\mathbf{P}^{1/2}\mathbf{\Gamma}\mathbf{P}^{1/2} = \mathbf{U}\mathbf{\Lambda}\mathbf{U}^H$, where $\mathbf{U}$ is a unitary matrix, and $\mathbf{\Lambda}$ is a diagonal matrix. It is shown in the Appendix that the overall estimator $\mathbf{G}_{opt}$ in (19) can be expressed as

$$\mathbf{G}_{opt} = \mathbf{Q}^{-1/2}\mathbf{V}\tilde{\mathbf{G}}_{opt}\mathbf{V}^H\mathbf{Q}^{-1/2} \tag{24}$$

where $\mathbf{V} = \mathrm{diag}(\mathbf{U}, \ldots, \mathbf{U})$, and $\tilde{\mathbf{G}}_{opt} = (\mathrm{E}[\tilde{\mathbf{z}}\tilde{\mathbf{z}}^H])^{-1}\,\mathrm{E}[\tilde{\mathbf{z}}\tilde{\mathbf{h}}^H(0)]$ acts on the transformed matched filter outputs $\tilde{\mathbf{z}} = [\tilde{\mathbf{z}}^T(-I)\cdots\tilde{\mathbf{z}}^T(I)]^T = \mathbf{V}^H\mathbf{Q}^{-1/2}\mathbf{z} = \tilde{\mathbf{h}} + \tilde{\mathbf{w}}$. $\tilde{\mathbf{G}}_{opt}$ is the MMSE estimator of the transformed channel coefficients $\tilde{\mathbf{h}}(0)$ from $\tilde{\mathbf{z}}$. Recall that $\mathbf{Q} = \mathrm{diag}(\mathbf{P}, \ldots, \mathbf{P})$, and thus, the transformation for each symbol takes the form $\tilde{\mathbf{z}}(i) = \mathbf{U}^H\mathbf{P}^{-1/2}\mathbf{z}(i)$. The matrix $\mathbf{Q}^{-1/2}$ whitens the noise $\mathbf{w}(i)$, and the unitary matrix $\mathbf{U}^H$ further decorrelates the transformed channel coefficients without affecting noise structure. Since $\{\tilde{\mathbf{z}}(i)\}$ are only correlated across symbols, the structure of $\tilde{\mathbf{G}}_{opt}$ is similar to that in the orthogonal case; the (k, n)th component of $\tilde{\mathbf{h}}(0)$ can be estimated independently by processing $\tilde{\mathbf{z}}_{k,n} = [\tilde{z}_{k,n}(-I), \ldots, \tilde{z}_{k,n}(I)]^T$ via the estimator $\tilde{\mathbf{g}}_{k,n,opt}$

$$\begin{aligned} \hat{\tilde{h}}_{k,n}(0) &= \tilde{\mathbf{g}}_{k,n,opt}^H \tilde{\mathbf{z}}_{k,n} \\ \tilde{\mathbf{g}}_{k,n,opt} &= (\lambda_{k,n}\mathbf{R} + \sigma_p^2\mathbf{I})^{-1}\lambda_{k,n}\mathbf{r} \end{aligned} \tag{25}$$

where $\{\lambda_{-K,0}, \ldots, \lambda_{k,n}, \ldots, \lambda_{K,N}\}$ denote the diagonal terms of $\mathbf{\Lambda}$, $\mathbf{R} = \mathbf{R}_{0,0}$, and $\mathbf{r} = \mathbf{r}_{0,0}$. Note that the form of the estimator in (25) is identical to the estimator in (20) under the assumption of identical temporal correlation structure for different channel components.

Due to the Toeplitz structure of $\mathbf{R}$, the estimator (24) also admits a frequency domain representation for large I, which is illustrated in Fig. 2. Note that the pre and postprocessing in Fig. 2 is in terms of $\mathbf{P}$ and $\mathbf{U}$ since $\mathbf{Q} = \mathrm{diag}(\mathbf{P}, \ldots, \mathbf{P})$ and $\mathbf{V} = \mathrm{diag}(\mathbf{U}, \ldots, \mathbf{U})$. $S(\nu)$ is the PSD associated with $r(m)$: $S(\nu) = \sum_{m=-\infty}^{+\infty} r(m) e^{-j2\pi m\nu}$. The different vector components in Fig. 2 are uncorrelated after the preprocessing by $\mathbf{P}^{-1/2}\mathbf{U}^H$. $\mathbf{P}$ is completely determined by the basis waveforms $\mathbf{u}(t)$, and $\mathbf{U}$ depends on $\mathbf{P}$ and the channel statistics $\mathbf{\Gamma}$.

C. Suboptimal Uniform Averager

We have shown that the optimal MMSE estimator can be decomposed into a bank of independent estimators [see (20) and

[4]This *delay/frequency separability* of the spreading function is assumed in other works as well, see, e.g., [18].

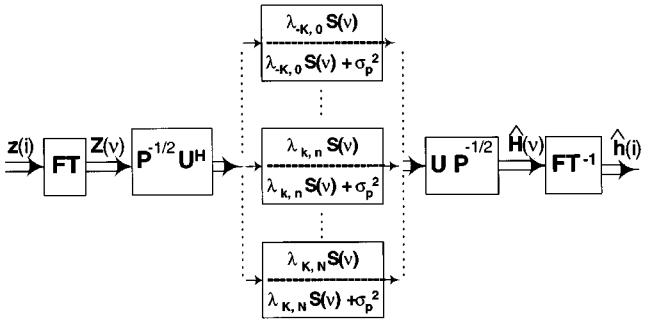

Fig. 2. Frequency-domain representation of the optimum estimator in the case of a nonorthogonal basis. The Fourier transform acts in time on $\{\mathbf{z}(i)\}$. $\mathbf{P}^{-1/2}\mathbf{U}^H$ and $\mathbf{U}\mathbf{P}^{-1/2}$ act on the different vector components.

(25)]: one for each multipath-Doppler channel coefficient (or transformed coefficient in the nonorthogonal case). The optimal estimator requires knowledge of channel statistics and involves a matrix inversion. We also propose a simple suboptimum uniform averaging estimator that is easy to implement:

$$\mathbf{g}_{unif} = a_{unif}\mathbf{1} \tag{26}$$

where $\mathbf{1} = [1, 1, \ldots, 1]^T$. Note that $\mathbf{g}_{unif}$ performs a uniform averaging of the $(2I+1)$ matched-filter outputs. For comparison with the optimal estimator, a_{unif} is chosen to minimize the MSE and is given by $a_{unif} = (\mathbf{r}_{k,n}^H \mathbf{1}/\mathbf{1}^H(\mathbf{R}_{k,n} + \sigma_p^2\mathbf{I})\mathbf{1})$. Note that the actual value of $a_{unif}(>0)$ is not important for bit detection in the case of linear receivers.

IV. Estimator Performance

In this section, we analyze the performance of the proposed estimators under various conditions. Our results demonstrate that the simple uniform averaging delivers near-optimal performance for proper choice of frame length I. We also provide guidelines for choosing I in practice.

We analyze the orthogonal-basis case without loss of generality. Furthermore, due to the decoupling between different channel components, we analyze the estimator for a particular component and drop the subscript (k, n). The MMSE associated with the optimal estimator $\mathbf{g}_{opt}$ for a given component is

$$\sigma_e^2 = \mathrm{E}\left[\,|h(0) - \mathbf{g}_{opt}^H\mathbf{z}|^2\right] \tag{27}$$

$$= r(0)\left[1 - \frac{1}{r(0)}\,\mathbf{r}^H(\mathbf{R} + \sigma_p^2\mathbf{I})^{-1}\mathbf{r}\right] \tag{28}$$

$$= r(0)\left[1 - \frac{1}{r(0)}\int_{-TB_d}^{TB_d} \frac{S^2(\nu)}{S(\nu) + \sigma_p^2}\,d\nu\right] \tag{29}$$

where the last equality holds in the limit of large I. To get an insight into the effect of Δt_c and σ_p^2 on the MMSE, we consider the simple case of an "idealized" uniform Doppler spectrum, that is, $S(\nu) = S_o$ for $\nu \in [-TB_d, TB_d]$. It can be readily shown that in this case, σ_e^2 reduces to

$$\sigma_{e,\,ideal}^2 = \frac{r(0)}{1 + \mathrm{SNR}^{eff}} \tag{30}$$

where

$$\mathrm{SNR}^{eff} = \frac{r(0)}{\sigma_p^2 2TB_d} \approx \frac{r(0)\Delta t_c}{\sigma_p^2 T} = \mathrm{SNR}^{pilot}\frac{\Delta t_c}{T} \tag{31}$$

and we have used the approximate relation $\Delta t_c \approx 1/2B_d$ between coherence time and Doppler spread [2]. The estimator performance in this idealized case is characterized by the effective SNR (SNR^{eff}) that is the product of the pilot SNR $\mathrm{SNR}^{pilot} = r(0)/\sigma_p^2$ and the normalized coherence time $\Delta t_c/T$. As is evident from (30), $\sigma_{e,\,ideal}^2$ is a monotonically decreasing function of SNR^{eff}. Thus, as $\Delta t_c/T$ increases, SNR^{eff} increases, resulting in reduced $\sigma_{e,\,ideal}^2$, which is consistent with the fact that larger $\Delta t_c/T$ enables averaging over more symbols to reduce the effects of noise. The idealized expression (30) is very useful in practical design since it requires minimal information about the channel [$r(0)$ and Δt_c]. In particular, as shown next, it can be appropriately calibrated to mimic the true MMSE in (29) fairly accurately.

We now present some numerical results to illustrate the utility of the idealized MMSE expression (30) and to compare the performance of $\mathbf{g}_{opt}$ and $\mathbf{g}_{unif}$ in a single-path channel. For all numerical simulations in this paper, the time-varying channel is simulated using the Jakes Model [1], [19] corresponding to a data rate of 2500 Hz and a carrier frequency of 1.8 GHz.[5] We consider a spread-spectrum system with a spreading gain of 64. Four samples per chip (256 samples per symbol) are used to simulate the signals. A randomly generated binary spreading code is used in the simulations for the pilot channel. The MSE can be computed analytically for $\mathbf{g}_{opt}$ via (28) and for $\mathbf{g}_{unif}$ via (32). For the numerical results, the theoretical MSE is computed via these two expressions by using statistics estimated directly from the Jakes model.

Fig. 3 illustrates the use of the idealized MMSE expression (30) for assessing the performance of optimal estimator. Fig. 3(a) shows three curves for $\sigma_{e,\,ideal}^2$ as a function of SNR^{eff}. The solid curve corresponds to (30). The dashed curve corresponds to a calibrated version of (30) to match the true MMSE in (28) of the optimum estimator at 30 km/h, which is computed using Jakes statistics. The calibration is done by scaling SNR^{eff} in (30) with an appropriate constant. [The true MMSE of $\mathbf{g}_{opt}$ as well as the calibrated idealized curve at 30 km/h are plotted in Fig. 3(b) for reference.] The asterisk curve in Fig. 3(a) corresponds to further scaling SNR^{eff} in the calibrated (dashed) curve by the factor 30/80 to yield an idealized curve for predicting the performance at 80 km/h. Fig. 3(b) compares the theoretical performance of $\mathbf{g}_{opt}$ at 80 km/h, based on Jakes model statistics, with the predicted performance in Fig. 3(a) (the asterisk curve). Note that the true performance of $\mathbf{g}_{opt}$ at 80 km/h is approximated fairly accurately by the predicted curve.

Fig. 4 compares the theoretical and simulated performance of $\mathbf{g}_{opt}$ and $\mathbf{g}_{unif}$ ($I = 5$) at a speed of 80 km/h. Theoretical MSE is computed analytically using Jakes statistics via (28) and (32), and simulated MSE is computed by directly averaging the

[5]The low data rate and relatively high speeds in some cases are chosen to emphasize Doppler effects. Time-selective signaling schemes that use sufficiently long, overlapping symbols [20], [21] may be used to induce such Doppler effects under realistic data rates and fading conditions.

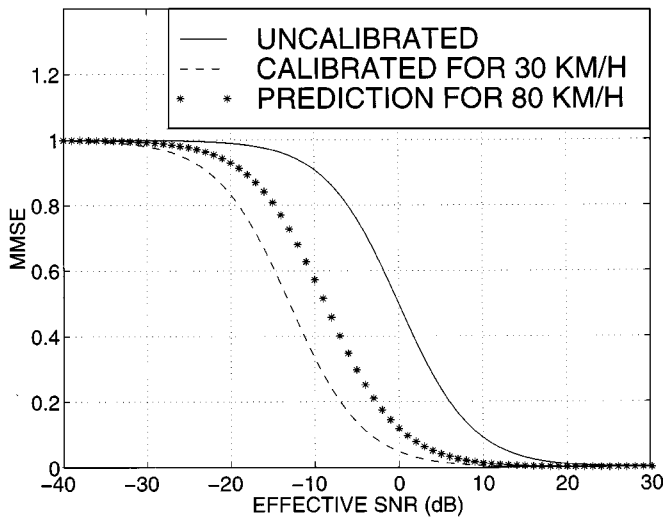

(a)

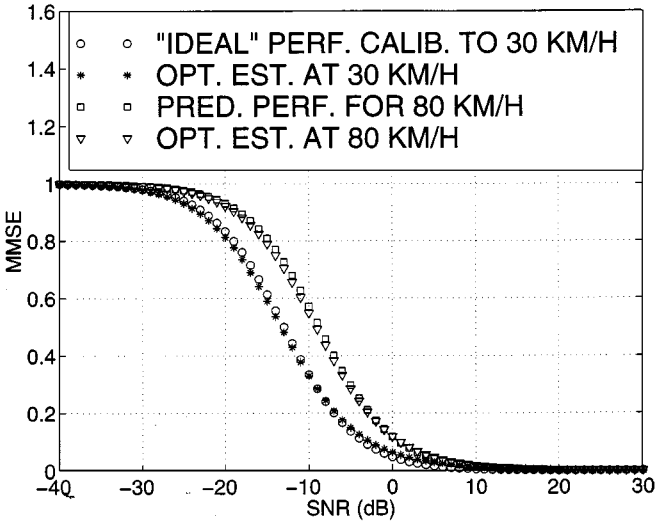

(b)

Fig. 3. (a) Optimal estimator MMSE curves based on the idealized flat spectrum approximation in (30). (b) Comparison between the true theoretical performance of $\mathbf{g}_{opt}$ and its predicted performance at 80 km/h ($TB_d = 0.05$) based on the calibrated idealized curve in (a).

estimator MSE over 50 000 symbols. Note that simulated and theoretical curves are virtually indistinguishable, demonstrating close agreement. However, the performance of $\mathbf{g}_{unif}$ is slightly degraded compared with $\mathbf{g}_{opt}$ due to mismatch of I with Δt_c (smaller I yields near-optimal performance).

We now investigate the dependence of the MSE of $\mathbf{g}_{unif}$ on I to guide its design. The MMSE of $\mathbf{g}_{unif}$ (using optimum a_{unif}) can be expressed as

$$\begin{aligned}\sigma^2_{e,\,unif}(I) &= \mathrm{E}[|h(0) - \mathbf{g}^H_{unif}\mathbf{z}|^2] \\ &= r(0)\left[1 - \frac{1}{r(0)}\,\frac{\left(\sum_{i=-I}^{I} r(i)\right)^2}{\sum_{i=-I}^{I}\sum_{j=-I}^{I} r(i-j) + (2I+1)\sigma_p^2}\right].\end{aligned} \tag{32}$$

For the idealized flat spectrum, (32) becomes

$$\begin{aligned}\sigma^2_{e,\,ideal,\,unif}(I) &= r(0)\left[1 - \frac{1}{2TB_d}\right. \\ &\left.\cdot\,\frac{\left(\int_{-TB_d}^{TB_d} \frac{\sin[\pi\nu'(2I+1)]}{\sin(\pi\nu')}\,d\nu'\right)^2}{\int_{-TB_d}^{TB_d}\left(\frac{\sin[\pi\nu'(2I+1)]}{\sin(\pi\nu')}\right)^2 d\nu' + (2I+1)/\mathrm{SNR}^{pilot}}\right].\end{aligned} \tag{33}$$

Note that $\sigma^2_{e,\,ideal,\,unif}$ in (33) does not depend on detailed channel statistics; it only depends on SNR^{pilot}, TB_d, and I and can thus be readily computed. Fig. 5 plots $\sigma^2_{e,\,ideal,\,unif}$ as a function of the frame length $(2I+1)$ for three different values of TB_d: 0.02 (30 km/h), 0.1 (150 km/h), and 0.2 (300 km/h). We note that the optimum frame size depends on both TB_d and

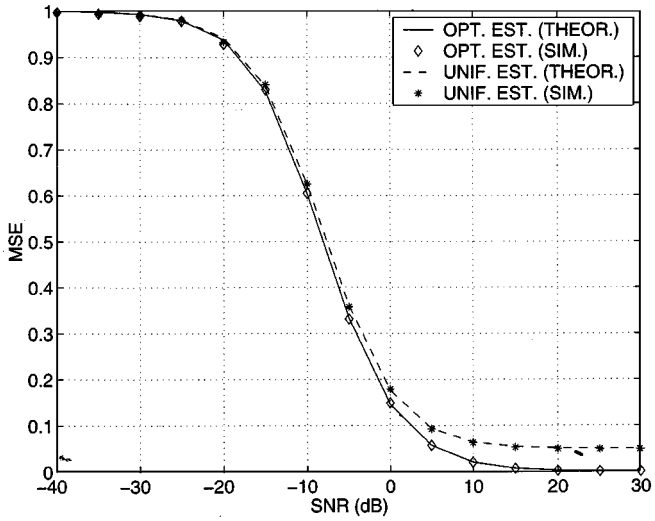

Fig. 4. Comparison of theoretical and simulated performance of $\mathbf{g}_{opt}$ and $\mathbf{g}_{unif}$ (frame length 11; $I = 5$) at 80 km/h ($TB_d = 0.05$). The continuous lines are the theoretical curves, and the marked points correspond to simulation data points. The theoretical and simulated data points are virtually indistinguishable.

SNR^{pilot}. Furthermore, the sensitivity of $\sigma^2_{e,\,ideal,\,unif}$ around the optimum frame size as well as is value increases with TB_d.[6]

Fig. 6 compares the performance of $\mathbf{g}_{opt}$ with that of $\mathbf{g}_{unif}$ as a function of SNR^{pilot} for two values of TB_d: 0.1 and 0.2. The lengths of the uniform averager are chosen using the plots in Fig. 5. We use the best lengths for the uniform averager at both 10 dB and 20 dB SNR for comparison. Using Fig. 5(b), the best length for $TB_d = 0.1$ is approximately 5 at 10 dB SNR and 3 at 20 dB SNR. Similarly, from Fig. 5(c), the best length for $TB_d = 0.2$ is approximately 3 at 10 dB SNR and 1 at 20 dB SNR. We note that the MSE of $\mathbf{g}_{unif}$ is very close to that of $\mathbf{g}_{opt}$, particularly at the SNR for which the length is optimum.[7] This

[6]Similar observations are reported in [16].

[7]Note also in Fig. 6 that, as expected, $\mathbf{g}_{unif}$ with longer length performs better at lower SNRs, whereas it performs better at high SNRs with short length.

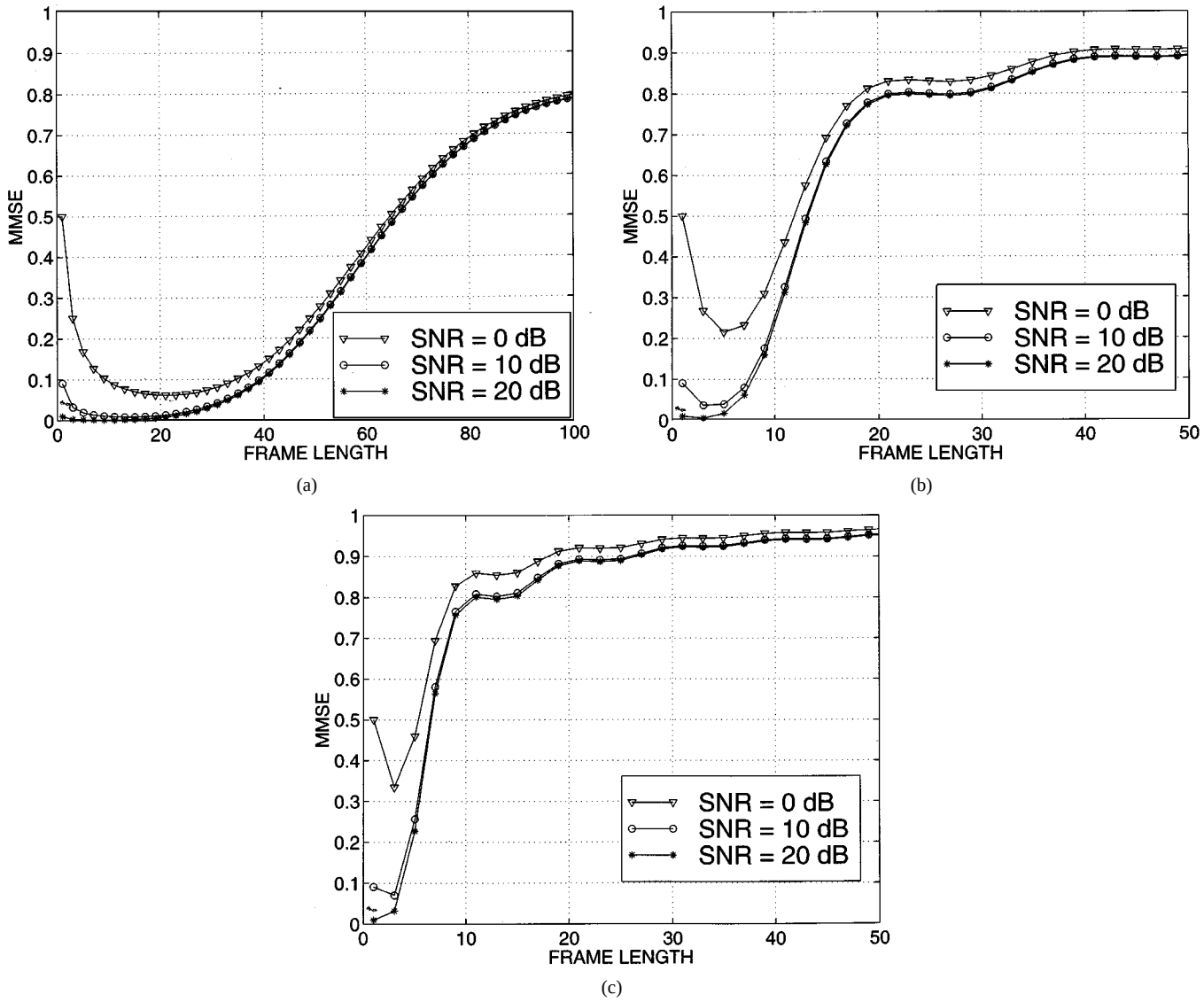

Fig. 5. Idealized MSE of the uniform averager [see (33)] as a function of the frame length $(2I+1)$. (a) $TB_d = 0.02$ (30 km/h). (b) $TB_d = 0.1$ (150 km/h). (c) $TB_d = 0.2$ (300 km/h).

shows that for an appropriate choice of I, the uniform averager can deliver near-optimal performance. Furthermore, the choice of I can be based on the idealized MSE expression given in (33), which only depends on TB_d and SNR^{pilot}. The optimum values of I for $\mathbf{g}_{unif}$ identified here are used in the next section to compare the overall receiver performance based on the two estimators.

V. Impact of Channel Estimation Errors on Receiver Performance

The receiver considered in our analysis exploits joint multipath-Doppler diversity via a time-frequency RAKE structure [5]. In contrast to results reported in the literature for the conventional RAKE, our results show that channel variations that are fast fading do not always impair receiver performance when a time–frequency (TF-)RAKE receiver is used. In fact, the receiver performance is determined by two *competing* effects under fast fading: *degradation* in channel estimation and *improvement* in inherent receiver performance due to Doppler diversity. At sufficiently high pilot SNRs, Doppler diversity effects can dominate, resulting in improved performance.

We consider binary phase-shift keying (BPSK) as the signaling scheme. The channel coefficients $\{h_{k,n}\}$ are estimated via a pilot signal corresponding to a particular spreading code. Simultaneously, data bits are transmitted over the same channel via a different spreading code.[8] The PSDs of the AWGN in the pilot and data channels are denoted by σ_p^2 and σ_d^2, respectively, with the corresponding SNRs given by $\text{SNR}^{pilot} = \text{E}[\|\mathbf{h}\|^2]/\sigma_p^2$ and $\text{SNR}^{data} = \text{E}[\|\mathbf{h}\|^2]/\sigma_d^2$. For simplicity, we ignore the interference between the pilot and data signals—interference suppression techniques tailored to our framework can be readily incorporated [22], [23]. We also assume orthonormal basis waveforms for both the pilot and data signals. Finally, under our assumption of negligible

[8]It can be shown that $\{h_{k,n}\}$ associated with two different codes with the same time-bandwidth product are nearly identical if they encounter the same propagation channel [5], [6].

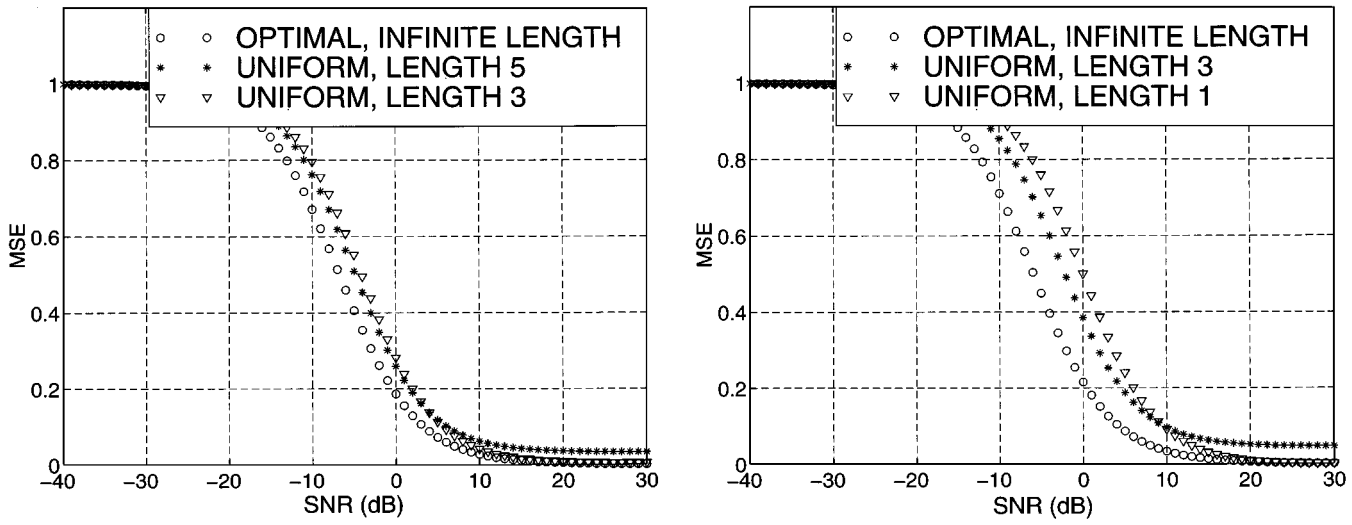

(a) (b)

Fig. 6. Comparison of the $\mathbf{g}_{opt}$ ($I = \infty$) and $\mathbf{g}_{unif}$ with appropriately chosen frame length based on Fig. 5. (a) $TB_d = 0.1$. (b) $TB_d = 0.2$.

intersymbol interference (ISI), the "one-shot detector," which decodes each symbol independently, suffices. We consider the detection of the 0th bit without loss of generality.

The output of the matched filters for the data signal is

$$\mathbf{z}_d = b_d\mathbf{h} + \mathbf{w}_d \tag{34}$$

where $\mathbf{w}_d$ is zero-mean AWGN with covariance matrix $\sigma_d^2\mathbf{I}$. The maximum-ratio-combiner (MRC) detector based on estimated channel coefficients is

$$\begin{aligned}\hat{b}_d &= \text{sign}\left(\text{real}\left\{\hat{\mathbf{h}}^H\mathbf{z}_d\right\}\right)\\ &= \text{sign}\left(\text{real}\left\{\sum_{n=0}^{N}\sum_{k=-K}^{K}\hat{h}_{k,n}^{*}z_{d,k,n}\right\}\right).\end{aligned} \tag{35}$$

Let $C = \text{real}(\hat{\mathbf{h}}^H\mathbf{z}_d)$ denote the decision statistic. Assuming that $b_d = 1$ is transmitted, the BEP is $P_e = \Pr(C < 0)$.

Exact calculation of P_e in the presence of channel estimation errors is fairly complicated if not intractable. We provide an estimate of P_e based on some simplifying assumptions that are supported with simulation results. Conditioned on a particular value of $h_{k,n}$, we model the corresponding estimated $\hat{h}_{k,n}$ as a Gaussian random variable

$$\hat{h}_{k,n} = h_{k,n} + e_{k,n} \tag{36}$$

where $e_{k,n}$ is zero-mean Gaussian with variance $\sigma_{e,k,n}^2$ corresponding to the MSE of the channel estimator.[9] The BEP conditioned on $\{h_{k,n}\}$ is given by[10] [2]

$$P_e(\gamma) = Q\left(\sqrt{2\gamma}\right) \tag{37}$$

[9]Note that this model is strictly not correct since the channel estimate is biased in general. However, assuming the error to be Gaussian is not unreasonable since the estimator is linear, and the noise is Gaussian.

[10]$Q(x) = (1/\sqrt{2\pi})\int_x^\infty e^{-u^2/2}\,du$.

where the γ is the conditional SNR per bit given by

$$\gamma = \frac{\left(\text{E}\left[\hat{\mathbf{h}}^H\mathbf{z}_d\right]\right)^2}{\text{var}\left[\hat{\mathbf{h}}^H\mathbf{z}_d\right]} = \frac{(\|\mathbf{h}\|^2)^2}{\mathbf{h}^H\mathbf{R}_e\mathbf{h} + \|\mathbf{h}\|^2\sigma_d^2 + \sigma_d^2\,\text{tr}(\mathbf{R}_e)} \tag{38}$$

where $\mathbf{R}_e = \text{E}[\mathbf{e}\mathbf{e}^H] = \text{diag}\{\sigma_{e,k,n}^2\}$ is the diagonal error covariance matrix. We make two approximations to facilitate analysis. First, we replace the quadratic form $\mathbf{h}^H\mathbf{R}_e\mathbf{h} = \sum_{n,k}|h_{k,n}|^2\sigma_{e,k,n}^2$ by its upper bound $\|\mathbf{h}\|^2\sigma_{e,\max}^2$, where $\sigma_{e,\max}^2 = \max\{\sigma_{e,k,n}^2\}$. Second, we assume that the product $\sigma_d^2\,\text{tr}(\mathbf{R}_e)$ is negligible compared with the other terms in the denominator of (38). With these approximations, we have

$$\gamma \approx \frac{\|\mathbf{h}\|^2}{\sigma_{e,\max}^2 + \sigma_d^2} = \sum_{k=-K}^{K}\sum_{n=0}^{N}\gamma_{k,n}, \quad \gamma_{k,n} = \frac{|h_{k,n}|^2}{\sigma_{e,\max}^2 + \sigma_d^2} \tag{39}$$

where $\gamma_{k,n}$ is the conditional SNR per bit for the (k, n)th channel component. This approximate system is equivalent to BPSK communication over a Rayleigh fading channel with $(N+1)(2K+1)$ level diversity and AWGN of variance $\sigma_{e,\max}^2 + \sigma_d^2$ [2]. The average SNR per bit for different channel components is $\overline{\gamma}_{k,n} = \text{E}[\gamma_{k,n}] = r_{k,n}(0)/(\sigma_{e,\max}^2 + \sigma_d^2)$. Using the expression $Q(x) = (1/\pi)\int_0^{\pi/2}\exp(-(x^2/2\sin^2(\theta)))\,d\theta$ [24], the conditional BEP in (37) can be averaged over the statistics of $\mathbf{h}$ to yield [24]

$$P_e = \frac{1}{\pi}\int_0^{\pi/2}\prod_{k=-K}^{K}\prod_{n=0}^{N}\left(1 + \frac{\overline{\gamma}_{k,n}}{\sin^2(\theta)}\right)^{-1}d\theta. \tag{40}$$

A. Numerical Results

We now present some numerical examples to illustrate the impact of Δt_c, the pilot and data SNRs, and level of diversity on the overall receiver performance with estimated channel coefficients. As noted earlier, the performance of the TF-RAKE

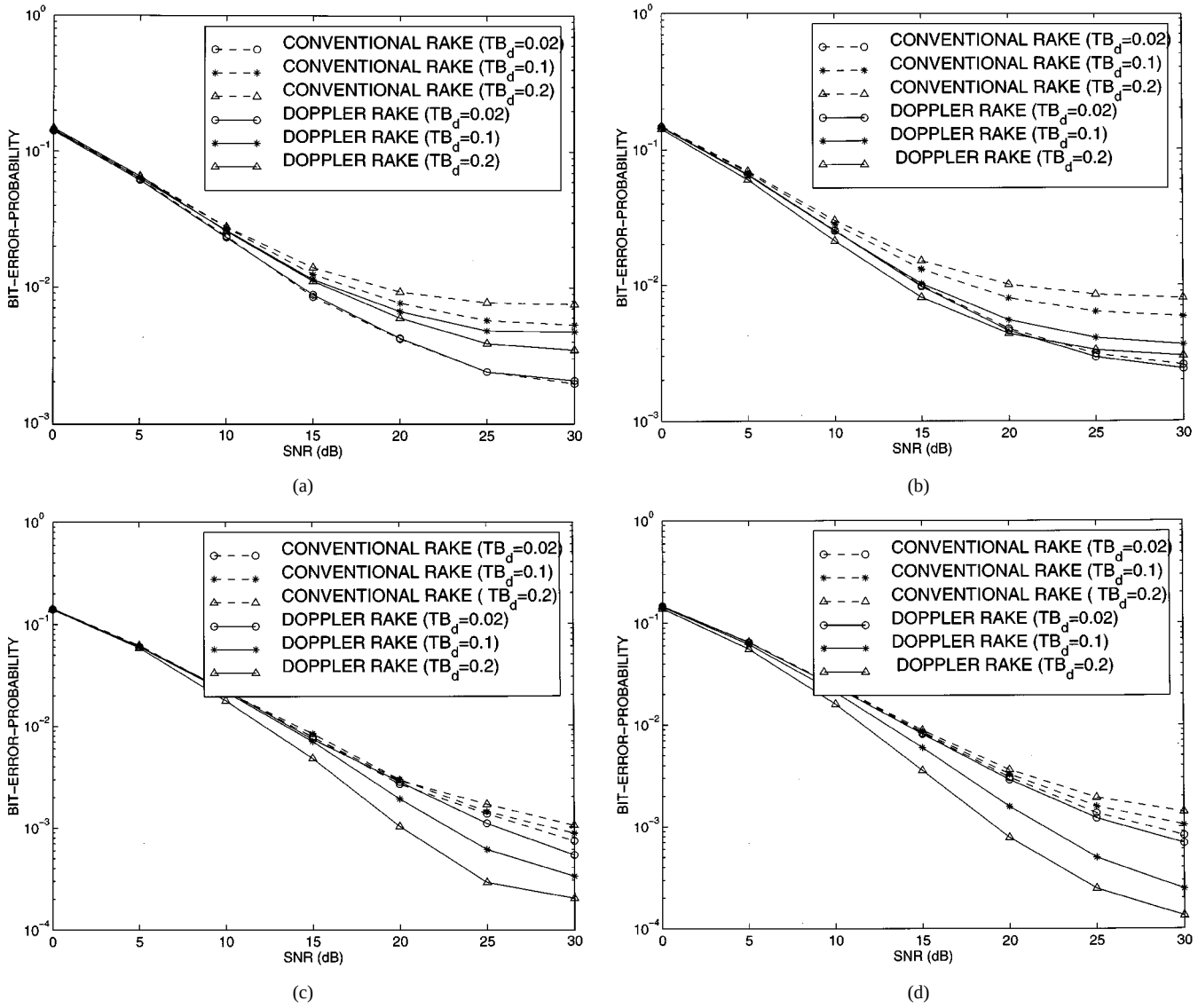

Fig. 7. Comparison of conventional and TF-RAKE receivers using the optimum channel estimator. (a) Simulated performance at $\text{SNR}^{pilot} = 10$ dB. (b) Theoretical performance at $\text{SNR}^{pilot} = 10$ dB. (c) Simulated performance at $\text{SNR}^{pilot} = 20$ dB. (d) Theoretical performance at $\text{SNR}^{pilot} = 20$ dB.

is governed by two opposing effects; as TB_d increases, the inherent receiver performance improves due to Doppler diversity, whereas channel estimation degrades. We consider the practical situation where $TB_d \leq 0.2$ so that the level of Doppler diversity is at most 3 ($K = 1$). The performance gain due to Doppler diversity depends on the ratio of the power in the $k = -1$ or $k = 1$ Doppler components to the total power in the three components [5]. For a flat Doppler spectrum, this ratio can be computed as [5]

$$\rho(TB_d) = \frac{\int_{-TB_d}^{TB_d} \text{sinc}^2(\beta - 1)\, d\beta}{\int_{-TB_d}^{TB_d} \text{sinc}^2(\beta)\, d\beta + 2\int_{-TB_d}^{TB_d} \text{sinc}^2(\beta - 1)\, d\beta}. \tag{41}$$

We note that the total channel power remains constant as TB_d varies; only the distribution of power over the components changes. As TB_d increases (shorter Δt_c) ρ increases, and the diversity gain increases.

We study receiver performance in the single-path case ($N = 0$). We compare two receivers: a conventional RAKE that does not exploit Doppler diversity and a TF-RAKE receiver that exploits joint multipath-Doppler diversity [5].[11] The two receivers are compared for the same type of channel estimator (optimal or uniform averager).

The performance of the conventional and TF RAKE receivers with optimum channel estimators is compared in Fig. 7. The comparison is made at three different values of TB_d (0.02, 0.1, 0.2) and two pilot SNRs: 10 and 20 dB. The optimum estimators are based on statistics estimated directly from the Jakes model. Fig. 7(a) compares the simulated performance (Monte Carlo averaging over 100 000 symbols) at $\text{SNR}^{pilot} = 10$ dB. The performance of the conventional RAKE progressively degrades with increasing TB_d due to errors in channel estimation. Similarly, the performance of the TF-RAKE degrades as TB_d increases from 0.02 to 0.1. However, its performance im-

[11]Note that there is no multipath diversity (single path) in our comparisons for the sake of simplicity.

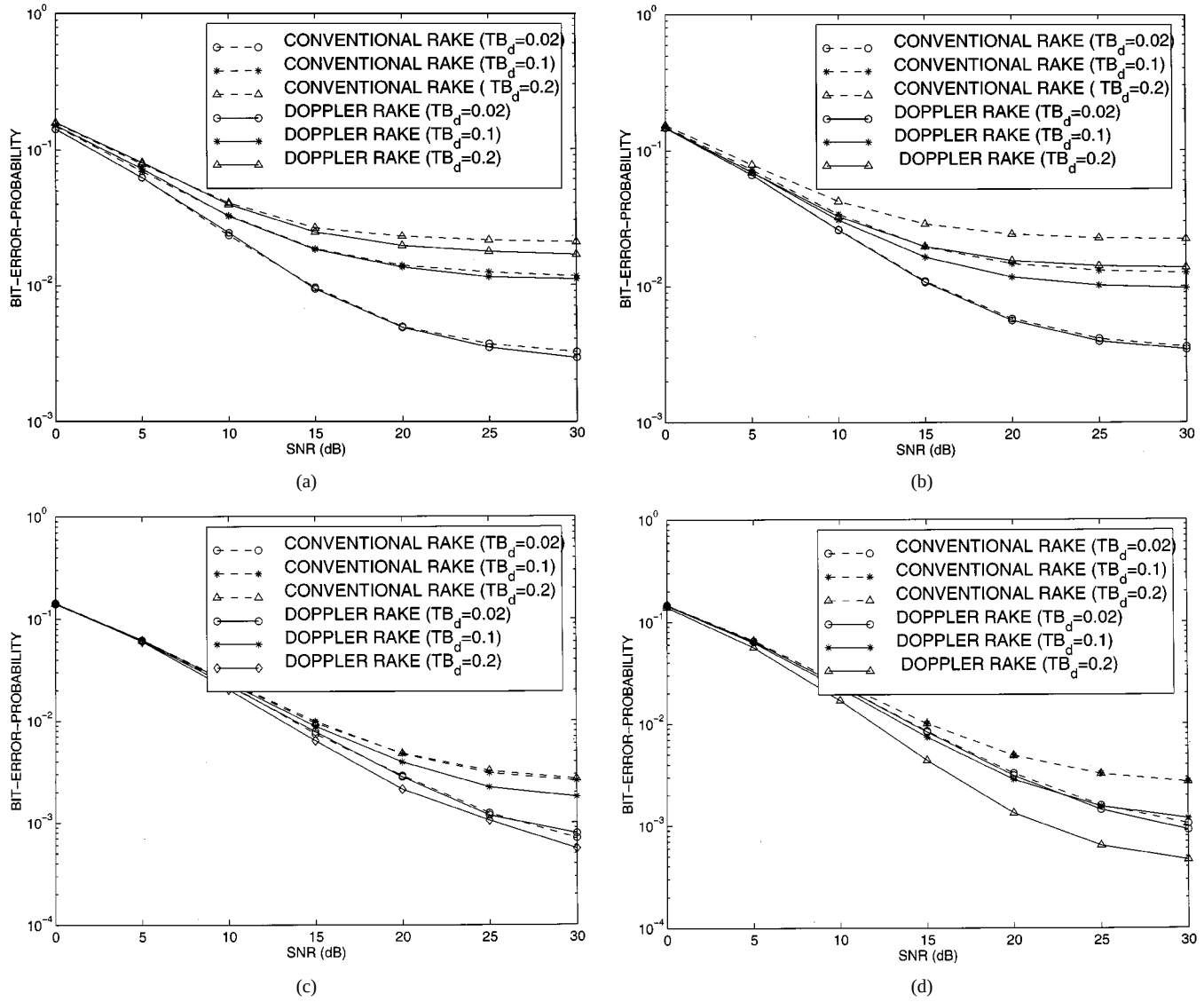

Fig. 8. Comparison of conventional and TF-RAKE receivers using the uniform averaging estimator. (a) Simulated performance at SNR^{pilot} = 10 dB. (b) Theoretical performance at SNR^{pilot} = 10 dB. (c) Simulated performance at SNR^{pilot} = 20 dB. (d) Theoretical performance at SNR^{pilot} = 20 dB.

proves relatively as TB_d increases from 0.1 to 0.2, indicating that the diversity effects dominate estimation error effects. On the whole, there is a net degradation in performance in going from $TB_d = 0.02$ to $TB_d = 0.2$. The corresponding comparison between the theoretical performance of the two receivers in Fig. 7(b) follows similar trends. However, the theoretical curves slightly overestimate the simulated performance in the case of the TF-RAKE receiver.

The plots in Fig. 7(c) and (d) show similar simulated/theoretical comparisons at SNR$^{pilot} = 20$ dB. In this case, the loss in performance of the RAKE with increasing TB_d is much less pronounced due to improved channel estimation. Similarly, the improvement in performance of the TF-RAKE is much more significant. It improves monotonically as TB_d is increased from $TB_d = 0.02$ to $TB_d = 0.2$, resulting in a net gain of about 7–8 dB at a BEP of 10^{-3}. The agreement between the simulated and theoretical curves is also closer in this case due to improved channel estimation. Note, however, that the performance of the receivers eventually saturates (BEP floors) as the data SNR is increased significantly beyond the pilot SNR (the beginning of that trend is evident from the plots).

Fig. 8 repeats the comparisons in Fig. 7 for receivers using the uniform averaging estimator. Using Fig. 5, the following frame lengths are used for the uniform averager at $TB_d = 0.02$, 0.1, and 0.2, respectively: 15 ($I = 7$), 5 ($I = 2$), and 3 ($I = 1$) at SNR$^{pilot} = 10$ dB; 9 ($I = 4$), 3 ($I = 1$), and 1 ($I = 0$) at SNR$^{pilot} = 20$ dB. At SNR$^{pilot} = 10$ dB, the simulated performance of the RAKE and TF-RAKE receivers is virtually identical, even though the theoretical comparison shows slightly better performance for the TF-RAKE. Overall, the performance degrades with increasing TB_d. On the other hand, at SNR$^{pilot} = 20$ dB, the performance of the TF-RAKE receiver first degrades as TB_d goes from 0.02 to 0.1 but then improves at $TB_d = 0.2$, yielding a slight net gain in performance relative to $TB_d = 0.02$. Nevertheless, the TF-RAKE performs significantly better than the conventional RAKE at $TB_d = 0.2$ since the latter suffers significantly due to channel estimation errors. The gains due to diversity dominate the loss due to estimation

errors in the TF-RAKE, resulting in significantly better performance compared with the conventional RAKE.

We conclude from Figs. 7 and 8 that with a reasonably strong pilot signal, the TF-RAKE using a simple uniform averaging estimator can significantly mitigate the BEP floors exhibited by the conventional RAKE under fast fading. On the other hand, a TF-RAKE armed with a better (MMSE) estimator not only provides resistance to BEP floors but can yield significant gains in performance due to Doppler diversity. We emphasize that the above comparison was based on a single path. The gains due to Doppler diversity will be relatively smaller in the presence of multipath due to diminishing gains with increasing diversity levels.

B. Asymptotic Performance for Large Number of Components

We now analyze the asymptotic behavior of P_e for a large number of channel components, which is analogous to the results reported in [25].[12] We assume that the total channel power $\sigma_h^2 = \mathrm{E}[\|\mathbf{h}\|^2]$ remains constant and is equally distributed among the different multipath-Doppler components. Thus, the decision statistic $C = \mathrm{real}(\hat{\mathbf{h}}^H \mathbf{z}_d) = \mathrm{real}(\sum_n \sum_k \hat{h}^*_{k,n} z_{d,k,n})$ is a sum of independent, identically distributed statistics $C_{k,n} = \hat{h}^*_{k,n} z_{d,k,n}$. Recalling that $\hat{h}_{k,n} = \mathbf{g}^H_{k,n,opt}\mathbf{z}_{k,n}$, with $\mathbf{g}_{k,n,opt}$ given by (20), the mean and variance of $C_{k,n}$ can be computed to be

$$\mathrm{E}[C_{k,n}] = \mathbf{r}^H \mathbf{g}_{opt} = r(0) - \sigma_e^2, \tag{42}$$

$$\begin{aligned}\mathrm{var}[C_{k,n}] &= \mathrm{E}[C_{k,n}][r(0) + \sigma_d^2] = (\mathbf{r}^H \mathbf{g}_{opt})[r(0) + \sigma_d^2] \\ &= [r(0) - \sigma_e^2][r(0) + \sigma_d^2]\end{aligned} \tag{43}$$

where $r(0)$ is the power in each channel component, and σ_e^2 is the MMSE in the estimate of the channel component. The second equalities above follow from (28). For a flat spectrum approximation, σ_e^2 is given by (30), and the above expressions can be further simplified to

$$\mathrm{E}[C_{k,n}] = \frac{r^2(0)\alpha}{1 + r(0)\alpha}, \quad \mathrm{var}[C_{k,n}] = \frac{r^2(0)\alpha}{1 + r(0)\alpha}\,[r(0) + \sigma_d^2] \tag{44}$$

where $\alpha = \Delta t_c / \sigma_p^2 T$. Let $M = (N+1)(2K+1)$. Then, $r(0) = \sigma_h^2/M$ and

$$\mathrm{E}[C] = \frac{\sigma_h^4 \alpha}{M + \sigma_h^2 \alpha}, \quad \mathrm{var}[C] = \frac{\sigma_h^4 \alpha}{2(M + \sigma_h^2 \alpha)}\,(\sigma_h^2/M + \sigma_d^2). \tag{45}$$

By applying the central limit theorem, it can be shown that as $M \to \infty$, $C' = \sqrt{M}\,C$ converges to a zero-mean Gaussian random variable with variance $\sigma_d^2 \sigma_h^4 \Delta t_c / 2\sigma_p^2 T > 0$. Consequently, $P_e = \Pr(C < 0) \to 0.5$ as the number of channel components (M) grows arbitrarily large. This shows that for any given pilot and data SNRs, the overall receiver performance eventually starts degrading as the number of diversity components increases. This is due to progressively significant errors in channel estimation since power in each component becomes vanishingly small.

[12]The number of multipath-Doppler components increases with TB for a fixed spread factor $T_m B_d$.

VI. Related Issues and Extensions

Here, we briefly discuss some related issues:

- another suboptimal estimator;
- extension to long codes;
- extension to multiuser systems;
- joint channel estimation and data detection.

In addition to the uniform averager, another suboptimal estimator that may be used in practice is the *correlation averager* $\mathbf{g}_{corr} = a_{corr}\mathbf{r}_{k,n}$, which performs a correlation-weighted averaging of the matched filter outputs. However, based on our simulation results (which are not reported here), a properly designed uniform averager performs as well as the correlation averager.

The framework presented in this paper can be readily extended to systems employing long codes—the key difference being that the optimal estimator becomes time-varying and, thus, imposes a higher computational complexity. In (10), the coefficients $\{h_{k,n}\}$ remain the same, but the basis functions change—the basis functions for the ith symbol are determined by the time–frequency shifted versions of the corresponding segment of the underlying long code. Consequently, the basis correlation matrix $\mathbf{P}$ in (15) and the estimator matrix $\mathbf{G}_{opt}$ in (19) are different, in general, for each symbol. From Fig. 2, we note that the additional computational burden is the eigendecomposition of the $(N+1)(2K+1) \times (N+1)(2K+1)$ matrix $\mathbf{P}^{1/2}\mathbf{\Gamma}\mathbf{P}^{1/2}$ for each symbol, which is not too stringent since $(N+1)(2K+1)$ is typically small. It is important to note that this symbol-by-symbol recomputation is only needed for oversampled systems employing long codes—there is no additional computation burden in the case of chip-rate sampled systems since $\mathbf{P} \approx \mathbf{I}$ in that case.

The channel estimators developed in this work can also be readily employed in multiuser systems. Essentially, an initial interference suppression stage is needed before the single-user estimator is applied. The interference suppression stage can be implemented either in a centralized [26] or a decentralized [22] fashion. In particular, the decentralized scheme in [22] uses projections onto basis functions of the form (8) that lie *outside* the channel spread to suppress the interference corrupting the information bearing signal within the channel spread. See [22] for more details.

Finally, while we addressed channel estimation and data detection separately, we now make a few comments to justify this approach by casting the problem in a joint fashion. Let

$$\mathbf{z}_p(i) = \mathbf{Q}_p \mathbf{h} + \mathbf{w}_p(i), \quad \mathbf{z}_d(i) = b(i)\mathbf{Q}_d \mathbf{h} + \mathbf{w}_d(i) \tag{46}$$

be the matched filter outputs for the pilot and data signals. Let $\mathbf{z}(i) = [\mathbf{z}_p^T(i)\ \mathbf{z}_d^T(i)]^T$. We are interested in decoding the bit vector $\mathbf{b} = [b(-I), \ldots, b(I)]^T$ from $\{\mathbf{z}(i)\colon i = -I, \ldots, I\}$. Consider maximum likelihood (ML) estimation of $\mathbf{b}$

$$\hat{\mathbf{b}} = \arg \max_{\mathbf{b} \in \{-1,1\}^N} p(\mathbf{z}|\mathbf{b}, \mathbf{h}, I) \tag{47}$$

where $p(\mathbf{z}|\mathbf{b}, \mathbf{h}, I)$ denotes the conditional density of $\mathbf{z}$ given $\mathbf{b}, \mathbf{h}$, and I. Since $\mathbf{h}$ constitutes nuisance parameters, we replace

it with its ML estimate, which can be shown to be

$$\hat{\mathbf{h}}_{ML} = \frac{1}{2I+1}(\mathbf{Q}_p + \mathbf{Q}_d)^{-1} \sum_{i=-I}^{I} [\mathbf{z}_p(i) + b(i)\mathbf{z}_d(i)]. \quad (48)$$

The bit detection problem becomes $\hat{\mathbf{b}} = \arg\max_{\mathbf{b}\in\{-1,1\}^N} p(\mathbf{z}|\mathbf{b}, \mathbf{h} = \hat{\mathbf{h}}_{ML}, I)$ using the compressed likelihood. Up to some additive constants the compressed log-likelihood is

$$\begin{aligned} &L(\mathbf{z}; \mathbf{b}, I) \\ &= \log(p(\mathbf{z}|\mathbf{b}, \mathbf{h} = \hat{\mathbf{h}}_{ML}, I)) \\ &= c + \frac{1}{2I+1} \sum_{i=-I}^{I} \sum_{j=-I}^{I} b(i)b(j)\mathbf{z}_d^H(i)(\mathbf{Q}_p + \mathbf{Q}_d)^{-1}\mathbf{z}_d(j) \\ &\quad + \frac{2}{2I+1} \text{real} \left[\sum_{i=-I}^{I} \sum_{j=-I}^{I} b(i)\mathbf{z}_d^H(i)(\mathbf{Q}_p + \mathbf{Q}_d)^{-1}\mathbf{z}_p(j) \right] \end{aligned} \quad (49)$$

where c represents a component that does not depend on $\mathbf{b}$. The above expression is analogous to the log-likehood of an interference channel, where the second term represents the interference between symbols. However, if the powers corresponding to different symbols are comparable (which is the case here), then the interference term may be neglected (and lumped into background noise), as is done in the use of the matched-filter receiver in conventional CDMA systems. Ignoring the interference term in (49), we arrive at the following (decoupled) bit decisions that maximize the compressed log-likelihood

$$\begin{aligned} \hat{b}(i) &= \text{sign}\left\{\text{real}\left[\mathbf{z}_d^H(i)(\mathbf{Q}_p + \mathbf{Q}_d)^{-1}\overline{\mathbf{z}_p}\right]\right\} \\ &\qquad i = -I, \ldots, I \\ \overline{\mathbf{z}_p} &= \frac{1}{2I+1} \sum_{j=-I}^{I} \mathbf{z}_p(j). \end{aligned} \quad (50)$$

The above detector is an MRC of the form (35), which uses $\hat{\mathbf{h}} = (\mathbf{Q}_p + \mathbf{Q}_d)^{-1}\overline{\mathbf{z}_p}$ as the channel estimate. This estimate essentially corresponds to the uniform averager since we are assuming that the channel remains constant over the frame. However, the constant-channel assumption was made only to give a simple argument to justify our decoupled approach to channel estimation and bit detection. The optimal estimator does better than the uniform averaging in (50) since it accounts for channel variations within the frame.

VII. Conclusion

We have addressed pilot-based linear MMSE estimation of time-varying multipath channels and its impact on coherent receiver performance. A critical channel characteristic controlling system performance is the coherence time, which is inversely proportional to the Doppler spread B_d. We have shown that the MMSE estimator admits a simple characterization in terms of a bank of filters. The estimator performance is governed by an effective SNR, which is the product of the pilot SNR and the normalized coherence time. An "idealized" MMSE curve based on the effective SNR is proposed for practical design. While the optimal estimator requires knowledge of channel statistics, our results demonstrate that a uniform averaging estimator of appropriate length can deliver near-optimal performance—the length can be chosen based on the "idealized" design curves.

We show that there are two competing effects controlling overall receiver performance: degradation in channel estimation versus improvement in inherent receiver performance (due to Doppler diversity) under faster fading. Our results demonstrate that Doppler diversity can be fruitfully exploited via a time–frequency RAKE receiver for mitigating BEP floors exhibited by the conventional RAKE under fast fading. We note that Doppler diversity gains are not directly attainable under practical fading conditions since TB_d is typically not large enough. However, time-selective signaling schemes that use longer (possibly overlapping) symbols (see, e.g., [21]) may be used to achieve desired values of TB_d (≈0.2) in practice.

Appendix

We derive (24) for the MMSE estimator in the case of a nonorthogonal basis. The optimal estimator (19) can be written as

$$\mathbf{G}_{opt} = \mathbf{Q}^{-1/2}(\mathbf{Q}^{1/2}E[\mathbf{h}\mathbf{h}^H]\mathbf{Q}^{1/2} + \sigma_p^2\mathbf{I})^{-1}\mathbf{Q}^{1/2}E[\mathbf{h}\mathbf{h}^H(0)]. \quad (51)$$

Under (23), we have $E[\mathbf{h}\mathbf{h}^H] = \mathbf{R}\otimes\mathbf{\Gamma}$ and $E[\mathbf{h}\mathbf{h}^H(0)] = \mathbf{r}\otimes\mathbf{\Gamma}$, where $\mathbf{R} = \mathbf{R}_{0,0}$, $\mathbf{r} = \mathbf{r}_{0,0}$, and $\otimes$ denotes the Kronecker product [27]. Thus, (51) can be equivalently expressed as

$$\begin{aligned} \mathbf{G}_{opt} &= \mathbf{Q}^{-1/2}(\mathbf{Q}^{1/2}(\mathbf{R}\otimes\mathbf{\Gamma})\mathbf{Q}^{1/2} + \sigma_p^2\mathbf{I})^{-1}\mathbf{Q}^{1/2}(\mathbf{r}\otimes\mathbf{\Gamma}) \\ &= \mathbf{Q}^{-1/2}(\mathbf{R}\otimes(\mathbf{P}^{1/2}\mathbf{\Gamma}\mathbf{P}^{1/2}) + \sigma_p^2\mathbf{I})^{-1}\mathbf{Q}^{1/2}(\mathbf{r}\otimes\mathbf{\Gamma}) \end{aligned} \quad (52)$$

where the second equality follows from the fact that $\mathbf{Q}^{1/2} = \text{diag}(\mathbf{P}^{1/2}, \ldots, \mathbf{P}^{1/2})$. Using the eigendecomposition $\mathbf{P}^{1/2}\mathbf{\Gamma}\mathbf{P}^{1/2} = \mathbf{U}\mathbf{\Lambda}\mathbf{U}^H$, we have

$$\begin{aligned} \mathbf{G}_{opt} &= \mathbf{Q}^{-1/2}(\mathbf{R}\otimes(\mathbf{U}\mathbf{\Lambda}\mathbf{U}^H) + \sigma_p^2\mathbf{I})^{-1}\mathbf{Q}^{1/2}(\mathbf{r}\otimes\mathbf{\Gamma}) \\ &= \mathbf{Q}^{-1/2}\mathbf{V}(\mathbf{R}\otimes\mathbf{\Lambda} + \sigma_p^2\mathbf{I})^{-1}\mathbf{V}^H\mathbf{Q}^{1/2}(\mathbf{r}\otimes\mathbf{\Gamma}) \end{aligned} \quad (53)$$

where $\mathbf{V} = \text{diag}(\mathbf{U}, \ldots, \mathbf{U})$ in the second equality, and we use the fact that $\mathbf{V}$ is unitary since $\mathbf{U}$ is unitary. Using the eigendecomposition, we also have

$$\begin{aligned} \mathbf{V}^H\mathbf{Q}^{1/2}(\mathbf{r}\otimes\mathbf{\Gamma}) &= \mathbf{r}\otimes(\mathbf{U}^H\mathbf{P}^{1/2}\mathbf{\Gamma}) = \mathbf{r}\otimes(\mathbf{\Lambda}\mathbf{U}^H\mathbf{P}^{-1/2}) \\ &= (\mathbf{r}\otimes\mathbf{\Lambda})\mathbf{V}\mathbf{Q}^{-1/2}. \end{aligned} \quad (54)$$

By substituting (54) in (53), we arrive at the following expression for $\mathbf{G}_{opt}$:

$$\mathbf{G}_{opt} = \mathbf{Q}^{-1/2}\mathbf{V}(\mathbf{R}\otimes\mathbf{\Lambda} + \sigma_p^2\mathbf{I})^{-1}(\mathbf{r}\otimes\mathbf{\Lambda})\mathbf{V}^H\mathbf{Q}^{-1/2} \quad (55)$$

which can be interpreted as follows. Consider the transformed vector $\tilde{\mathbf{z}} = \mathbf{V}^H\mathbf{Q}^{-1/2}\mathbf{z}$, which results in $\tilde{\mathbf{z}}(i) = \mathbf{U}^H\mathbf{P}^{-1/2}\mathbf{z}(i) = \tilde{\mathbf{h}}(i) + \tilde{\mathbf{w}}(i)$, where $\mathrm{E}[\tilde{\mathbf{w}}(i)\tilde{\mathbf{w}}(i')^H] =$

$\sigma_p^2\mathbf{I}\delta_{i-i'}$, and $\mathrm{E}[\tilde{\mathbf{h}}(i)\tilde{\mathbf{h}}^H(i')] = r(i-j)\mathbf{\Lambda}$. The linear MMSE estimator of $\tilde{\mathbf{h}}(0)$ from $\tilde{\mathbf{z}}$ is given by

$$\begin{aligned}\tilde{\mathbf{G}}_{opt} &= \left(\mathrm{E}\left[\tilde{\mathbf{z}}\tilde{\mathbf{z}}^H\right]\right)^{-1}\mathrm{E}\left[\tilde{\mathbf{z}}\tilde{\mathbf{h}}^H(0)\right] \\ &= \left(\mathbf{R}\otimes\mathbf{\Lambda}+\sigma_p^2\mathbf{I}\right)^{-1}(\mathbf{r}\otimes\mathbf{\Lambda}) \qquad (56)\end{aligned}$$

and thus, (55) can be expressed as $\mathbf{G}_{opt} = \mathbf{Q}^{-1/2}\mathbf{V}\tilde{\mathbf{G}}_{opt}\mathbf{V}^H\mathbf{Q}^{-1/2}$, which is precisely the form in (24).

REFERENCES

[1] T. S. Rappaport, *Wireless Communications*. Englewood Cliffs, NJ: Prentice-Hall, 1996.

[2] J. G. Proakis, *Digitial Communications*, 3rd ed. New York: McGraw-Hill, 1995.

[3] T. Ojanperä and R. Prasad, "An overview of air interface multiple access for IMT-2000/UMTS," *IEEE Commun. Mag.*, vol. 36, pp. 82–95, Sept. 1998.

[4] E. Dahlman, B. Gudmundson, M. Nilsson, and J. Skold, "UMTS/IMT-2000 based wideband CDMA," *IEEE Commun. Mag.*, vol. 36, pp. 70–80, Sept. 1998.

[5] A. M. Sayeed and B. Aazhang, "Joint multipath-Doppler diversity in mobile wireless communications," *IEEE Trans. Commun.*, vol. 47, pp. 123–132, Jan. 1999.

[6] P. A. Bello, "Characterization of randomly time-variant linear channels," *IEEE Trans. Commun. Syst.*, vol. COM-11, pp. 360–393, Nov. 1963.

[7] T. Kailath, "Sampling models for linear time-variant filters," Res. Lab. Electron., Mass. INst. Tecnol., Cambridge, MA, Tech. Rep. 352, May 1959.

[8] R. Kennedy, *Fading Dispersive Communication Channels*. New York: Wiley, 1969.

[9] G. B. Giannakis and C. Tepedelenlioglu, "Basis expansion models and diversity techniques for blind identification and equalization of time-varying channels," *Proc. IEEE (Special Issue on Blind System Identification and Estimation)*, vol. 86, pp. 1969–1986, Oct. 1998.

[10] A. W. Fuxjaeger and R. A. Iltis, "Adaptive parameter estimation using parallel Kalman filtering for spread spectrum code and Doppler tracking," *IEEE Trans. Commun.*, vol. 42, pp. 2227–2230, June 1994.

[11] ——, "Acquisition of timing and Doppler-shift in a direct sequence spread-spectrum system," *IEEE Trans. Commun.*, vol. 42, pp. 2870–2880, June 1994.

[12] J. K. Cavers, "An analysis of pilot symbol assisted modulation for Rayleigh fading channels," *IEEE Trans. Veh. Technol.*, vol. 40, pp. 689–693, Nov. 1991.

[13] H. Andoh, M. Sawahashi, and F. Adachi, "Channel estimation using time multiplexed pilot symbols for coherent Rake combining for DS-CDMA mobile radio," in *Proc. PIMRC*, 1997, pp. 954–958.

[14] F. Ling, "Coherent detection with reference-symbol based estimation for direct sequence CDMA uplink communication," in *Proc. Veh. Technol. Conf.*, 1993, pp. 400–403.

[15] B. Sklar, "Rayleigh fading channels in mobile digital communication system Part II: Mitigation," *IEEE Commun. Mag.*, pp. 103–109, July 1997.

[16] M. Benthin and K. Kammeyer, "Influence of channel estimation on the performance of a coherent DS-CDMA system," *IEEE Trans. Vehic. Technol.*, vol. 46, pp. 262–268, May 1997.

[17] R. M. Gray, "On the asymptotic eigenvalue distribution of Toeplitz matrices," *IEEE Trans. Inform. Theory*, vol. IT-18, pp. 725–730, Nov. 1972.

[18] J. S. Sadowsky and V. Kafedziski, "On the correlation and scattering functions of the WSSUS channel for mobile communications," *IEEE Trans. Veh. Technol.*, vol. 47, pp. 270–282, Feb. 1998.

[19] W. C. Jakes, "Mobile radio propagation," in *Microwave Mobile Communications*, W. C. Jakes, Ed. New York: Wiley, 1974, pp. 11–78.

[20] S. Bhashyam, A. M. Sayeed, and B. Aazhang, "Time-selective signaling and reception for multipath fading channels," in *Proc. IEEE Int. Symp. Inform. Theory*, 1998, p. 157.

[21] ——, "Time-selective signaling and reception for communication over multipath fading channels," *IEEE Trans. Commun.*, vol. 48, pp. 83–94, Jan. 2000.

[22] T. A. Kadous and A. M. Sayeed, "Decentralized multiuser detection for time-varying multipath channels," *IEEE Trans. Commun.*, vol. 48, pp. 1840–1852, Nov. 2000.

[23] T. Kadous and A. M. Sayeed, "Progressively powerful multiuser detector for rapidly time-varying multipath environments," in *Proc. Globecom*, 1999.

[24] M. K. Simon and M.-S. Alouini, "A unified approach to the performance analysis of digital communication over generalized fading channels," *Proc. IEEE*, vol. 86, pp. 1860–1877, Sept. 1998.

[25] E. Telatar and D. Tse, "Capacity and mutual information of wideband multipath fading channels," *IEEE Trans. Inform. Theory*, pp. 1384–1400, July 2000.

[26] A. M. Sayeed, A. Sendonaris, and B. Aazhang, "Multiuser detection in fast fading multipath environments," *IEEE J. Select. Areas Commun.*, vol. 16, pp. 1691–1701, Dec. 1998.

[27] J. W. Brewer, "Kronecker products and matrix calculus in system theory," *IEEE Trans. Circuits Syst.*, vol. CAS-25, pp. 772–781, Sept. 1978.

Marc-Antoine R. Baissas received the degree in electrical and computer engineering from the Grandes Ecoles SUPELEC, Paris, France, and the M.S. degree in electrical engineering from the University of Wisconsin, Madison.

While at the University of Wisconsin, he conducted research in statistical signal processing and wireless communications. After receiving the M.S. degree, he joined Texas Instruments, Inc., Dallas, TX, in 1999.

Akbar M. Sayeed (S'89–M'97) received the B.S. degree from the University of Wisconsin, Madison (UWM), in 1991 and the M.S. and Ph.D. degrees in 1993 and 1996, respectively, from the University of Illinois at Urbana-Champaign, all in electrical and computer engineering.

While at the University of Illinois, he was a Research Assistant with the Coordinated Science Laboratory and was also the Schlumberger Fellow in signal processing from 1992 to 1995. From 1996 to 1997, he was a Postdoctoral Fellow at Rice University, Houston, TX. Since August 1997, he has been with UWM, where he is currently an Assistant Professor with the Electrical and Computer Engineering Department. His research interests are in wireless communications, statistical signal processing, wavelets, and time–frequency analysis.

Dr. Sayeed received the NSF CAREER Award in 1999 and the ONR Young Investigator Award in 2001. He is currently serving as an Associate Editor for the IEEE SIGNAL PROCESSING LETTERS.